Adsorption-induced reversible colloidal aggregation

B. M. Law,[1] J.-M. Petit,[2] and D. Beysens[2]
[1]*Condensed Matter Laboratory, Department of Physics, Kansas State University, Manhattan, Kansas 66506-2601*
[2]*CEA, Département de Recherche Fondamentale, sur la Matière Condensée, 38054 Grenoble Cedex 9, France*
(Received 29 September 1997)

Reversible colloidal aggregation in binary liquid mixtures has been studied for a number of years. As the phase separation temperature of the liquid mixture is approached the thickness of an adsorption layer around the colloidal particles increases. Beysens *et al.* [Phys. Rev. Lett. **54**, 2123 (1985); Ber. Bunsenges. Phys. Chem. **98**, 382 (1994)] have demonstrated experimentally that this adsorption layer is intimately connected with the aggregation of the colloidal particles; however, no definitive theory has been available that can explain all of the experimental observations. In a recent work [J.-M. Petit, B. M. Law, and D. Beysens, J. Colloid Interface Sci. (to be published)] we have extended and improved the Derjaguin-Landau-Verwey-Overbeek theory of colloidal aggregation [E. J. W. Verwey and J. Th. G. Overbeek, *Theory of the Stability of Lyophobic Colloids* (Elsevier, New York, 1948)] by taking into account the presence of an adsorption layer and by more realistically modeling the attractive dispersion interactions using the Dzyaloshinskii-Lifshitz-Pitaevskii theory [Adv. Phys. **10**, 165 (1961)]. In the present paper we apply this theory to a lutidine-water mixture containing a small volume fraction of silica colloidal particles. We demonstrate that the theory can quantitatively account for many of the experimentally observed features such as the characteristics of the aggregated state, the general shape of the aggregation line, and the temperature dependence of the second virial coefficient.
[S1063-651X(98)10605-0]

PACS number(s): 82.70.Dd, 82.65.Dp, 64.70.Ja, 05.40.+j

I. INTRODUCTION

Colloids and the dynamics of colloidal aggregation have been of continuing interest for many decades. Colloidal solutions and aggregates are extremely common (e.g., latex paints and soot) and are therefore of great fundamental and technological importance [1]. Colloidal particles are large in comparison to atoms and molecules; they can therefore be more readily imaged and studied. They have provided severe tests of our basic understanding of interacting particles [2], the dynamics of fractal and nonfractal aggregate growth [3], and the freezing and melting of (colloidal) crystals [4,5]. Most aggregation processes studied to date have been induced by either changing the *p*H of the colloidal solution or by adding salt to the colloidal solution [6]. In both cases the electrostatic repulsive interaction is significantly screened so that the attractive dispersion interactions dominate, thus causing aggregation. Frequently this aggregation process is irreversible. The colloidal particles stick and form a fractal aggregate; the particles are in point contact at the global minimum of the interaction energy. Reversible colloidal aggregation is a less common occurrence. In 1985 Beysens and Estève [7] observed thermally induced reversible colloidal aggregation in a homogeneous mixture of 2,6-lutidine plus water containing a dilute suspension of silica colloidal particles. Subsequent extensive studies of this system [8] and similar systems by many groups [9–11] have characterized a number of intriguing properties for this type of aggregation.

In Fig. 1 we schematically show the phase diagram and colloidal aggregation line for a mixture of 2,6-lutidine and water in the presence of a small volume fraction ($\sim 10^{-3}$) of silica or latex colloidal particles. The bold solid line on this diagram represents the two-phase coexistence curve for lutidine and water, which possesses a lower consolute point with a critical lutidine mass fraction m_c (≈ 0.29) and a critical temperature T_c ($\approx 34\,^{\circ}\mathrm{C}$). Below the coexistence curve the liquid mixture is in the one-phase region, while above the coexistence curve the liquid mixture phase separates into two phases, one lutidine rich and the other lutidine poor. The presence of the colloidal particles does not significantly alter the shape or position of the coexistence curve. The light solid line represents a typical colloidal aggregation line for the colloidal particles in this mixture. If the colloidal particles possess a small surface charge density $\sigma \sim 1-2\ \mu\mathrm{C/cm}^2$, the aggregation line appears on the lutidine-poor side of the phase diagram [Fig. 1(a)]. For such a system at fixed composition, as the temperature is increased towards the coexistence temperature T_{cx}, the colloidal particles acquire a lutidine-rich adsorption layer of thickness d, which thickens with increasing temperature [12]. At the aggregation temperature T_a the colloidal particles begin to aggregate and eventually, due to their greater density, fall out of the solution. The aggregation line represents the variation of T_a with lutidine mass fraction m_L. The aggregation line is asymmetric with respect to the critical composition (m_c) and for a number of systems is observed to extend to higher compositions than m_c [10]. Above the coexistence curve, in the two-phase region, Gallagher, Kurnaz, and Maher [9] have observed that colloidal particles of small charge density are primarily confined to the lutidine-rich phase with very few particles in the lutidine-poor phase. Additionally, the colloidal particles are not observed on the critical interface until a particular temperature, which they identify with the wetting temperature T_w. For $T \leqslant T_w$ the colloidal particles possess a zero contact angle with the critical interface. Above T_w the colloidal particles are always observed at the liquid-liquid interface and the contact angle is presumably finite.

The intimate connection between the presence of the ad-

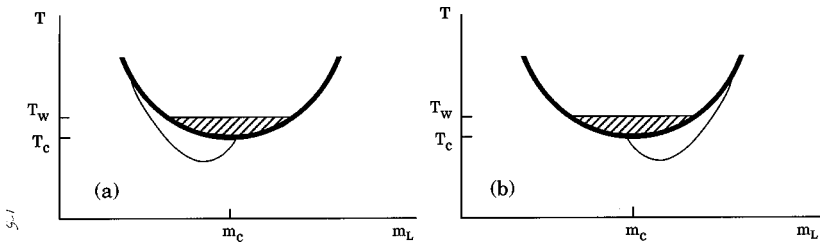

FIG. 1. Schematic phase diagram of the 2,6-lutidine plus water system with a small volume fraction of charged colloidal particles. The heavy solid line depicts the 2,6-lutidine and water coexistence curve with a lower critical consolute temperature $T_c \approx 34$ °C and critical mass fraction of lutidine $m_c \approx 0.29$. The light solid line demarcates the colloidal aggregation line. The colloidal particles aggregate for temperatures above this line. (a) Small colloidal surface charge density $\sigma \sim 1-2$ μC/cm^2. In the two-phase region the colloidal particles reside primarily in the lutidine-rich phase. Below the wetting temperature T_w (shaded region) no colloidal particles are observed at the critical liquid-liquid interface. (b) Large colloidal surface charge density $\sigma \sim 4$ μC/cm^2. Above the coexistence curve the colloidal particles now reside primarily in the water-rich phase.

sorption layer around the colloidal particles and the process of aggregation has been confirmed by studying the correlation between adsorption and aggregation with the addition of Mg^{2+} ions to the solution [13]. The process of aggregation was observed to disappear with the disappearance of the lutidine adsorption layer. Light scattering studies [14] suggest that liquidlike bonds hold the colloidal aggregate together, where each individual colloidal particle is free to rotate but where the center-to-center separation distance $r \sim 3R_c$ in the aggregated state [12]. R_c is the colloidal core radius. If a cluster of aggregated particles is quenched to a temperature below T_a the cluster has been observed to fragment back to individual colloidal particles [15]. Beysens *et al.* [8] have suggested that all of these observations are most consistent with the aggregated particles being situated in a secondary minimum of the interaction free energy rather than the global minimum that occurs at point contact.

For colloidal particles possessing a large surface charge density $\sigma \sim 4$ μC/cm^2, the aggregation line is found on the lutidine-rich side of the coexistence curve [Fig. 1(b)] and water is preferentially adsorbed around the colloidal particles [9]. In the two-phase region, above the coexistence curve, the colloidal particles now reside primarily in the water-rich phase.

There have been numerous theoretical papers proposing possible explanations for this thermally induced reversible colloidal aggregation. The various proposed physical origins for the aggregation phenomenon have included prewetting [16], capillary condensation [16], a percolation transition [17], critical fluctuations [18], and a three-component phase separation [19]. Unfortunately, most of these explanations have not provided definitive predictions that could be compared directly with experimental results.

In a recent work [21] we outlined a theory for adsorption-induced aggregation that possesses many of the experimental features. In this paper we compare this theory explicitly with experiment. The experimental observations have noted an interconnection between the presence of an adsorption layer and the process of reversible colloidal aggregation in certain binary liquid mixtures. Light scattering measurements monitoring the development of the aggregate have determined that the dynamics follows the conventional Smoluchowski dynamics of a compact object [14]. The growth process therefore resembles in many respects the Derjaguin-Landau-Verwey-Overbeek (DLVO) [22] theory of colloidal aggregation, but induced in some manner by the presence of an adsorbed layer. In the usual DLVO theory of aggregation colloidal particles begin to aggregate when the repulsive electrostatic potential is partially or totally dominated by the attractive dispersion interaction. Under certain circumstances, for partial domination, a secondary minimum can form in the total free energy as a function of distance and the colloidal particles aggregate into a secondary minimum provided a large repulsive barrier still inhibits the colloidal particles from aggregating to the global minimum that occurs at point contact [20]. The aggregates in this secondary minimum are held together weakly and they can frequently be redispersed into the suspension by a reversal of the solution conditions. If the attractive dispersion interaction totally dominates the repulsive electrostatic potential, the colloidal particles aggregate to the global minimum in the free energy that occurs at point contact; the aggregates stick to each other irreversibly and can never be redispersed into solution. The formation of a secondary minimum, which frequently leads to reversible aggregation, is normally induced by increasing the salt concentration or by decreasing the surface potential.

The effect of an adsorption layer on the total interaction potential has never been taken into account in the DLVO theory. In [21] we have therefore modified and improved the DLVO theory to include the presence of an adsorbed layer around the colloidal particles. We have also replaced the approximate Hamaker representation of the attractive interaction by the more accurate Dzyaloshinskii-Lifshitz-Pitaevskii (DLP) theory of dispersion forces [23], which is known to give a more accurate representation of the attractive interaction in real systems. We have found that under certain circumstances the adsorption layer reduces the repulsive electrostatic potential and above a certain adsorption layer thickness the colloidal particles aggregate. When the adsorption layers of two colloidal particles touch and coalesce the colloidal particles are situated in an ''adsorption bubble'' of different composition from the bulk. The different bubble composition possesses a different Debye screening length from the bulk mixture and the colloids ''feel'' a large repulsion inside the adsorption bubble, which prevents aggregation to the global minimum. This aggregation mechanism is rather different from the secondary minimum idea [20] in the normal DLVO theory. Before proceeding to describe this theory for the interaction potential in more detail

(Sec. III) we first summarize the colloidal aggregation dynamics that obeys the generalized Smoluchowki diffusion equation (Sec. II). In Sec. IV we consider the 2,6-lutidine plus water system in the presence of silica colloidal particles. The colloidal solution parameters are defined in Sec. IV A, the aggregation dynamics at fixed composition are considered in Sec. IV B, the aggregation line is examined in Sec. IV C, and finally the second virial coefficient is discussed in Sec. IV D. The paper concludes with a summary and discussion of our results (Sec. V).

II. COLLOIDAL AGGREGATION DYNAMICS

If c_s represents the initial number density of particles of monomer radius R_1 and $F(r)$ is the two-particle interaction potential at separation distance r, then the variation in the density of particles c as a function of time and position is described by the generalized Smoluchowski diffusion equation [24]

$$\frac{\partial c}{\partial t}=\frac{1}{r^2}\frac{\partial}{\partial r}r^2\left(D_{11}\frac{\partial c}{\partial r}+\frac{D_{11}c}{k_BT}\frac{dF}{dr}\right). \tag{1}$$

In the approximation where the mutual diffusion coefficient D_{11} is given by the diffusion coefficient of two identical freely diffusing particles $D_{11}=D_{11}^{\infty}=2D_1$. In the initial stages of aggregation all particles have the same radius R_1 and $D_1=k_BT/6\pi\mu R_1$, where μ is the solution viscosity. In the stationary approximation ($\partial c/\partial t=0$), which occurs after a relaxation time $t\approx R_1^2/D_{11}^{\infty}$ ($\sim$10 ms in our case), and in the absence of interactions [$F(r)=0$] the particles aggregate solely via diffusion. Equation (1) can then readily be integrated once to derive the number of particles diffusing through any closed surface towards a central particle [25]

$$J=4\pi D_{11}^{\infty}R_1c_s. \tag{2}$$

If the particles coalesce on contact, the rate of decrease in the number density (c) of particles is then given by [25]

$$-\frac{dc}{dt}=4\pi D_{11}^{\infty}R_1c^2. \tag{3}$$

Equation (3) describes only the initial decrease in the number of particles, each of size R_1. At later times cluster-cluster aggregation can occur and Eq. (3) must be generalized to describe the formation of clusters of k particles with density c_k,

$$\frac{dc_k}{dt}=\frac{1}{2}\sum_{\substack{i=1\\ j=k-i}}^{j=k-1}K(i,j)c_ic_j-c_k\sum_{i=1}^{\infty}K(i,k)c_i, \tag{4}$$

where $i+j=k$ and the kernel $K(i,j)$ represents the rate coefficient for a specific clustering mechanism between clusters of size i and j. The first term on the right-hand side corresponds to the formation of k-fold clusters from the coalescence of i- and j-fold clusters, while the second term represents the decrease in the number of k-fold clusters due to the coalescence of k-fold and j-fold clusters. Van Dongen and Ernst [26] have considered the properties of this equation for various general kernels $K(i,j)$. From Eqs. (3) and (4) the kernel describing Brownian aggregation is given by

$$K(i,j)=4\pi D_{ij}^{\infty}R_{ij}, \tag{5}$$

where $D_{ij}^{\infty}=D_i+D_j$ and the radius of interaction $R_{ij}\approx R_i+R_j$, with R_i the radius of the i-fold cluster. If the clusters are fractal with fractal dimension d_f then

$$R_i=R_1i^{1/d_f} \tag{6}$$

and

$$D_i=\frac{k_BT}{6\pi\mu R_1i^{1/d_f}}. \tag{7}$$

At late times (t) and for a large average cluster size $\overline{k}(t)$ Eq. (4) exhibits dynamic scaling [26]

$$c_k(t)\sim\overline{k}(t)^{-2}\phi\left(\frac{k}{\overline{k}(t)}\right), \tag{8}$$

where for the Brownian kernel [Eq. (5)] the function

$$\phi(z)\sim\exp(-Az) \tag{9}$$

for large z and A a constant. If $i\approx j$ the characteristic Brownian aggregation time is given by [25]

$$t_{Brown}=\frac{2}{K(1,1)c_s}=\frac{3\mu}{4k_BTc_s}. \tag{10}$$

This time corresponds to the time at which the total number of clusters of particles has decreased by one-half.

Thus far we have not taken into account the pair interaction potential $F(r)$ between colloidal particles. Normally $F(r)$ consists of a screened electrostatic repulsive potential for charged particles and an attractive dispersion energy due to correlated dielectric fluctuations [6]. If the repulsive potential is dominant the aggregation process can be significantly slower than the Brownian aggregation time t_{Brown}. The effects of $F(r)$ on the aggregation dynamics were discussed by Fuchs [27]. For real particles the mutual diffusion coefficient between two monomers D_{11} takes a more complicated form when the two colloidal particles are in close proximity. The particles diffuse towards each other more slowly the closer the colloidal particles are to one another because it becomes more difficult to push solvent molecules out of the way due to the confining effects of the colloidal particles themselves. This ''hydrodynamic interaction'' causes D_{11} to decrease with decreasing separation distance r relative to its value at infinite separation denoted by D_{11}^{∞} [24,28]. The specific expression for D_{11} [24] is complicated but can be readily evaluated numerically. The net effect of the pair potential and the hydrodynamic interaction on the dynamics of colloidal aggregation is to alter the aggregation time by the ''stability factor'' W [24],

$$t_{agg}=Wt_{Brown}, \tag{11}$$

where

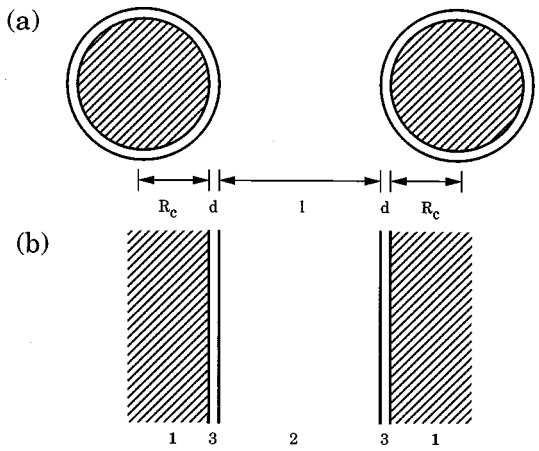

FIG. 2. (a) Schematic diagram of two interacting colloidal spheres of radius R_c, with an adsorbed layer of thickness d, separated by a distance l. (b) Schematic diagram of two semi-infinite planes 1, with adsorbed layers 3 of thickness d, separated by a medium 2 of thickness l.

$$W=2\int_2^{\infty}\frac{D_{11}^{\infty}}{D_{11}}\exp\left(\frac{F}{k_BT}\right)\frac{ds}{s^2} \tag{12}$$

and $s=r/R_1$. The form of the interaction potential $F(r)$ therefore plays a key role in determining the aggregation dynamics.

III. THE INTERACTION POTENTIAL $F(r)$

In another work [21] we have developed a theoretical model for the colloidal interaction potential $F(r)$ and how it is influenced by the presence of a pure lutidine layer of thickness d surrounding a charged colloidal particle in a lutidine plus water mixture. The model is more general than this specific example and could be applied to the influence of any type of adsorption layer on the general stability and characteristics of a colloidal solution where adsorption of a surface active minority component can occur. The primary factor that alters the colloidal dynamics is the different Debye screening lengths in the adsorbed layer and in the bulk solution. The Debye screening effect has the most influence on the behavior of the repulsive potential. The existence of this Debye length in the adsorbed layer is the cause for the reversible colloidal aggregation in the lutidine-water system as the adsorption thickness increases.

In Fig. 2(a) we show two colloidal particles with a pure lutidine layer of thickness d where the distance between the lutidine covered colloids is l and the center-to-center separation distance is $r=2R_c+2d+l$. In the figure the colloidal particles each have a core radius of R_c. The total free energy of the interaction is composed of a sum of three terms

$$F=F_{n=0}^{DLP}+F_{n>0}^{DLP}+F^{elec}, \tag{13}$$

where $F_{n=0}^{DLP}$ is the zero-frequency DLP dispersion interaction, $F_{n>0}^{DLP}$ is the finite-frequency DLP dispersion interaction, and F^{elec} is the screened electrostatic potential. Each colloidal particle has a surface charge density of σ and is screened by counterions. Only the terms $F_{n=0}^{DLP}$ and F^{elec} are influenced by this screening because the lowest frequency that enters the $F_{n>0}^{DLP}$ term, $\xi_1=3\times10^{14}$ Hz, is well above the response frequency of the heavy ions in solution.

In [21] we have demonstrated that to a good approximation these three terms are given by the following expressions. At zero frequency ($n=0$) the DLP dispersion interaction between two colloidal particles is given by

$$F_{n=0}^{DLP}(l)\approx\frac{k_BT}{8}H(l,R_c+d)A_{n=0}^{DLP}, \tag{14}$$

where the effective Hamaker constant $A_{n=0}^{DLP}$ is related to the DLP surface free energy $\mathcal{F}_{plane,n=0}^{DLP}$ between two planar semi-infinite surfaces by

$$A_{n=0}^{DLP}=\frac{8\pi l^2}{k_BT}\mathcal{F}_{plane,n=0}^{DLP}. \tag{15}$$

The geometric factor $H(l,R_c+d)$ in Eq. (14) has the form

$$H(a,b)=\frac{4b^2}{a(a+4b)}+\frac{4b^2}{(a+2b)^2}+2\ln\left[\frac{a(a+4b)}{(a+2b)^2}\right]. \tag{16}$$

As discussed in [21], the advantage of relating $F_{n=0}^{DLP}$ [depicted in Fig. 2(a)] to $\mathcal{F}_{plane,n=0}^{DLP}$ [depicted in Fig. 2(b)] through a geometric factor is that the effects of an adsorbed layer can more readily be incorporated into the term $\mathcal{F}_{plane,n=0}^{DLP}$. The approximation represented by Eq. (14) has been demonstrated to be accurate to within 10– 20% [29], which is sufficient for our requirements. For the two plane half spaces 1, each with an adsorbed layer 3 of thickness d, separated by medium 2 of thickness l,

$$\mathcal{F}_{plane,n=0}^{DLP}(l)=\frac{k_BT}{4\pi}\int_0^{+\infty}dyy\ \ln[1-\Delta_{21}^{e}(d)^2e^{-2s_2l}], \tag{17}$$

where

$$\Delta_{21}^{e}(d)=\frac{\Delta_{23}^{e}+\Delta_{31}^{e}e^{-2s_3d}}{1+\Delta_{23}^{e}\Delta_{31}^{e}e^{-2s_3d}}, \tag{18}$$

$$\Delta_{ij}^{e}=\frac{\epsilon_i(0)s_i-\epsilon_j(0)s_j}{\epsilon_i(0)s_i+\epsilon_j(0)s_j}, \tag{19}$$

and

$$s_i^2=y^2+\lambda_{Di}^{-2}. \tag{20}$$

The effects of ionic screening have been incorporated through the Debye screening length λ_{Di}, while the symbol $\epsilon_i(0)$ represents the static dielectric constant in medium i. Note that the Debye screening length in the adsorbed layer λ_{D3} will in general differ from the Debye screening length in the medium separating the colloidal particles λ_{D2}.

The finite-frequency ($n>0$) DLP dispersion interaction between two colloidal particles takes a similar form

$$F_{n>0}^{DLP}\approx\frac{k_BT}{8}H(l,R_c+d)A_{n>0}^{DLP}, \tag{21}$$

where the effective Hamaker constant $A_{n>0}^{DLP}$ and the free energy between two semi-infinite planar surfaces $\mathcal{F}_{plane,n>0}^{DLP}$ are related by an equation similar to Eq. (15),

$$A_{n>0}^{DLP}=\frac{8\pi l^2}{k_BT}\mathcal{F}_{plane,n>0}^{DLP}=\sum_{n=1}^{+\infty} I_n(\xi_n,l,d), \tag{22}$$

with

$$I_n(\xi_n,l,d)=\int_{b_n}^{+\infty} dx\; x\{\ln[1-\Delta_{21}^{-}(d)^2e^{-x}] + \ln[1-\Delta_{21}(d)^2e^{-x}]\}, \tag{23}$$

$$\Delta_{21}^{-}(d)=\frac{\Delta_{23}^{-}+\Delta_{31}^{-}\exp\left(-\frac{ds_3x}{lp}\right)}{1+\Delta_{23}^{-}\Delta_{31}^{-}\exp\left(-\frac{ds_3x}{lp}\right)}, \tag{24}$$

similarly for $\Delta_{21}(d)$, where

$$\Delta_{j'j}^{-}=\frac{\epsilon_{j'}s_j-\epsilon_j s_{j'}}{\epsilon_{j'}s_j+\epsilon_j s_{j'}},\quad \Delta_{j'j}=\frac{s_j-s_{j'}}{s_j+s_{j'}}, \tag{25}$$

$$s_j=\sqrt{p^2-1+\epsilon_j/\epsilon_2},\quad p=x/b_n, \tag{26}$$

$$\xi_n=n\frac{2\pi k_BT}{\hbar},\quad \xi_l=\frac{c}{2l\sqrt{\epsilon_2}},\quad b_n=\frac{\xi_n}{\xi_l}. \tag{27}$$

In these equations $\epsilon_j=\epsilon_j(i\xi_n)$ represents the frequency-dependent dielectric constant at the imaginary frequency $i\xi_n$ [30]. As noted above, the Debye screening length does not enter the expression for $F_{n>0}^{DLP}$.

For the situation depicted in Fig. 2(a) assuming a symmetric Z-Z electrolyte with a high surface charge density $\lambda_{D2},\lambda_{D3}\ll R_c$, the electrostatic repulsive free energy between the colloidal particles is given by [22]

$$F^{elec}=32\pi\epsilon_2(0)\epsilon_0R_c(k_BT\gamma/Ze)^2\ln[1+\exp(-l/\lambda_{D2})], \tag{28}$$

with

$$\gamma=\tanh[Ze\psi(d)/4k_BT], \tag{29}$$

where $\psi(d)$ is the potential at the interface between the adsorbed layer and the bulk medium [21]. To a good approximation

$$\psi(d)=\frac{2k_BT}{Ze}\ln\left(\frac{1+\tanh[Ze\psi(0)/4k_BT]\exp(-d/\lambda_{D3})}{1-\tanh[Ze\psi(0)/4k_BT]\exp(-d/\lambda_{D3})}\right), \tag{30}$$

where $\psi(0)$ is the surface potential at the surface between the colloidal particle and the adsorbed layer, which is related to the surface charge density σ by

$$\psi(0)=\mathrm{sgn}(\sigma)\frac{k_BT}{Ze}\cosh^{-1}\left(1+\frac{\sigma^2}{4n\epsilon_3(0)\epsilon_0k_BT}\right). \tag{31}$$

TABLE I. Dielectric parameters for silica and 2,6-lutidine.

Material	$\varepsilon(0)$	ε_{0+}	ε_{vis}	ω_{ir} (10^{14} rad/s)	ω_{uv} (10^{16} rad/s)
Silica[a]	3.81	3.81	2.098	1.88	2.033
Lutidine	7.33[b]	2.42[b]	2.177[c]	5.65[d]	1.39[e]

[a]Data taken from [30].
[b]Reference [56].
[c]Using the method of calculation in [32].
[d]The C-H stretch infrared frequency from [57].
[e]From a Cauchy plot using the data from [57].

The Debye screening lengths in the adsorbed layer and in the bulk medium are given, respectively, by

$$\lambda_{D3}=\sqrt{\frac{\epsilon_3(0)\epsilon_0k_BT}{2Z^2e^2n}} \tag{32}$$

and

$$\lambda_{D2}=\sqrt{\frac{\epsilon_2(0)\epsilon_0k_BT}{2Z^2e^2nf}}, \tag{33}$$

where nf is the anion or cation concentration in the solvent medium and n is the corresponding concentration in the adsorbed layer.

In the following section we will observe that the total free energy $F(r)$ not only plays an essential role in determining the aggregation behavior through the stability factor W [Eq. (12)] but is also important in determining the behavior of the second virial coefficient that describes corrections to the ideal gas behavior of the colloidal particles, below the aggregation temperature T_a.

IV. COMPARISON WITH EXPERIMENTS ON LUTIDINE PLUS WATER

In this section we will compare the theory of the previous sections with the experiments on charged colloidal silica particles in the system 2,6-lutidine plus water. This system has been the most well characterized and studied thus far.

A. Colloidal solution parameters

Many materials parameters are required in the calculation of $F(r)$ and W. The frequency-dependent dielectric constant is often modeled using the Ninham-Parsegian form [31]

$$\epsilon(i\xi)=1+\frac{\epsilon_{0+}-\epsilon_{vis}}{1+(\xi/\omega_{ir})^2}+\frac{\epsilon_{vis}-1}{1+(\xi/\omega_{uv})^2}, \tag{34}$$

where ω_{ir} and ω_{uv} represent the most important absorption frequencies in the infrared and ultraviolet range respectively, ϵ_{0+} is the dielectric constant in the far-infrared region, and ϵ_{vis} is a constant determined by a procedure given in [32]. The absorption frequency ω_{uv} can be estimated from the refractive index data at various wavelengths using a Cauchy plot [30,32]. In Table I we list the dielectric parameters for silica and for 2,6-lutidine. A similar but more general form is assumed for water [33]

TABLE II. Dielectric data for water taken from [58].

Microwave		Infrared			Ultraviolet		
ω_{MW} (10^{11} rad/s)	C_{MW}	ω_{ir} (10^{14} rad/s)	C_{ir}	γ_{ir} (10^{14} rad/s)	ω_{uv} (10^{16} rad/s)	C_{uv}	γ_{uv} (10^{16} rad/s)
0.9875	76.89	0.31904	1.42857	0.227	1.26098	0.03919	0.07748
		1.04828	0.73514	0.577	1.51925	0.05700	0.13369
		1.39771	0.15359	0.425	1.73195	0.09233	0.23396
		3.03851	0.14250	0.379	1.97503	0.15562	0.31144
		6.38087	0.07936	0.850	2.26369	0.15224	0.44969
					2.81062	0.27114	0.95105

$$\epsilon(i\xi)=1+\frac{C_1}{1+\xi/\omega_1}+\sum_{l=2}^{12}\frac{C_l}{1+(\xi/\omega_l)^2+\gamma_l\xi/\omega_l^2}. \quad (35)$$

The parameters C_l, ω_l, and γ_l are listed in Table II, where the oscillator strengths C_l must satisfy the zero-frequency sum rule

$$\epsilon(0)=1+C_1+\sum_{l=2}^{12}C_l=81 \quad (36)$$

for water.

The dielectric constant for a lutidine-water mixture $\epsilon_2(i\xi)$ at frequency ξ can be calculated from the lutidine $[\epsilon_L(i\xi)]$ and water $[\epsilon_W(i\xi)]$ dielectric constants using the Clausius-Mossotti equation [32]

$$f(\epsilon_2(i\xi))=\Omega[\phi_L f(\epsilon_L(i\xi))+(1-\phi_L)f(\epsilon_W(i\xi))], \quad (37)$$

where

$$f(x)=\frac{x-1}{x+2}, \quad (38)$$

ϕ_L is the volume fraction of lutidine, and the fractional volume change on mixing is assumed to be negligible ($\Omega=1$).

Numerous materials parameters are required in the calculation to describe the lutidine-water solution, the adsorption layer, and the colloidal particles. For convenience these parameters are collected in Table III; they will each be discussed at the appropriate time. For the viscosity of this mixture as a function of composition, required in the calculation of the Brownian diffusion time t_{Brown}, we have assumed a typical value of $\mu\sim 2.0$ cp at 30 °C [34], where we have ignored the temperature and composition dependences of the viscosity. The divergence of the viscosity due to critical fluctuations is in general quite small compared to the background viscosity [35].

The Stöber colloidal particles used by Beysens *et al.* in many of their experiments possess surface hydroxyl groups that undergo a surface dissociation in the lutidine-water mixture that leaves the surface negatively charged and releases a H^+ ion into solution. Lutidine (L) is a weak base because of the lone pair of electrons on the nitrogen group; the H^+ ions therefore hydrogen bond to the lutidine to form a complex ion $(CH_3)_2C_5H_3N{:}H^+$, which we will denote $L{:}H^+$ or more simply L^+. The pH for this solution is approximately constant (≈ 9.5) over a wide range of lutidine-water compositions for a small fixed colloidal volume fraction [36]. For water solutions the concentration product is always constant [37]

$$[H^+][OH^-]=10^{-14}\ \text{mole}^2\ \text{L}^{-2} \quad (39)$$

and therefore with a pH$=9.5$, $[H^+]=1.9\times 10^{17}$ ions/m^3 and $[OH^-]=1.9\times 10^{22}$ ions/m^3 and therefore by electrical neutrality $[L^+]=1.9\times 10^{22}$ ions/m^3. Hence the ion concentration in the bulk solution is

$$nf\approx[L^+]=[OH^-]=1.9\times 10^{22}\ \text{ions/m}^3, \quad (40)$$

independent of lutidine concentration. For a lutidine mass fraction $m_L=0.25$ the Debye screening length in the solution $\lambda_{D2}=31.2$ nm [Eq. (33)].

TABLE III. Material parameters used in this paper.

Solution parameters
- solution viscosity $\mu\sim 2.0$ cp at 30 °C [34]
- lutidine mass fraction $m_L=0.25$ (value assumed in Secs. IV B and IV D)
- temperature $T\approx T_c=307.15$ K
- pH$=9.5$ (independent of composition [36])
- ionic valence $Z=1$
- cation or anion concentration $nf\approx 1.9\times 10^{22}$ ions/m^3 (independent of composition)
- Debye screening length $\lambda_{D2}=31.2$ nm for $m_L=0.25$

Adsorption layer parameters
- lutidine volume fraction v_L(layer)$=1$ (assume)
- cation or anion concentration $n\approx 7.6\times 10^{22}$ ions/m^3 for $m_L=0.25$ and v_L(layer)$=1$
- Debye screening length $\lambda_{D3}=8.4$ nm for $m_L=0.25$ and v_L(layer) $=1$

Colloidal parameters
- colloidal radius $R_c\sim 100$ nm
- colloidal concentration $c_s\sim 5\times 10^{11}$ cm^{-3} (typical)
- surface charge density $\sigma\approx 0.1$ OH$^-$/nm^2 [59]
- fractal dimension $d_f=3$ [14]
- hard-sphere second virial coefficient $B_2=1\times 10^{10}$ mL/mole for $R_c=100$ nm
- Brownian aggregation time $t_{Brown}=3\mu/4k_BTc_s=0.7$ s
- stability factor assumed for aggregation $W=500$

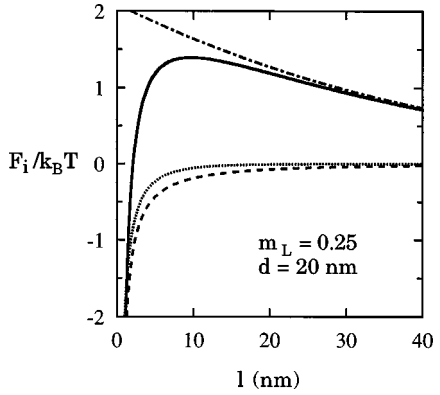

FIG. 3. Contributions to the colloidal interaction free energy F_i as a function of the separation distance l between two colloidal particles for $m_L=0.25$ and adsorption thickness $d=20$ nm, where $F_i=F$ (solid line), $F_{n=0}^{DLP}$ (dotted line), $F_{n>0}^{DLP}$ (dashed line), and F^{elec} (dash-dotted line).

The parameter f, which determines the ion concentration in the adsorbed layer, is difficult to measure. We will assume that

$$f=\frac{(\text{No. of moles of lutidine in mixture/unit vol})}{(\text{No. of moles of lutidine in layer/unit vol})} \quad (41)$$

$$=\frac{\phi_L(\text{mixture})}{\phi_L(\text{layer})}, \quad (42)$$

where ϕ_L is the volume fraction of lutidine and the second equality (42) can readily be proved. In this paper we generally assume that the adsorbed layer consists of pure lutidine and therefore $\phi_L(\text{layer})=1$; consequently the ion concentration in the adsorbed layer $n\approx 7.6\times 10^{22}$ ions/m^3 for $m_L=0.25$ and the Debye screening length in the lutidine adsorption layer $\lambda_{D3}=8.4$ nm [Eq. (32)].

B. The free energy of interaction and the aggregation dynamics at fixed composition

The various contributions to the total free energy can now readily be calculated from Eqs. (13)–(33). In this subsection we consider the free-energy contributions and the aggregation dynamics for a fixed lutidine mass fraction of $m_L=0.25$ and a fixed colloidal concentration of $c_s\sim 5\times 10^{11}$ cm^{-3}. These values are similar to those used in the experiments of Beysens *et al.* In Fig. 3 we show F, $F_{n=0}^{DLP}$, $F_{n>0}^{DLP}$, and F^{elec} as a function of l for $d=20$ nm. Previously we have demonstrated [21] that the dispersion energy terms $F_{n=0}^{DLP}$ and $F_{n>0}^{DLP}$ are not very sensitive to the value of d; in contrast, F^{elec} is extremely sensitive to the value of the adsorbed lutidine layer thickness d. In Fig. 4 we show the variation of F for a wide range in d where the variation is primarily determined by the behavior of F^{elec} with d. For small d (~ 5 nm) there is a very strong repulsive barrier that inhibits aggregation, while with increasing d this barrier progressively decreases until for $d=20$ nm the repulsive barrier has fallen to a peak barrier height of the order of the thermal energy k_BT and aggregation can readily occur.

For temperatures below the aggregation temperature T_a Gurfein, Beysens, and Perrot [12] used static light scattering

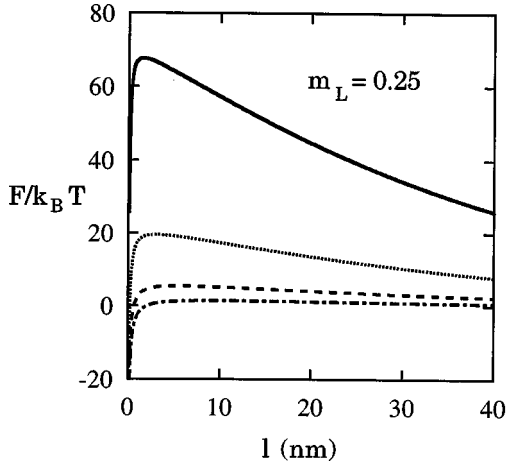

FIG. 4. Variation of the total colloidal free energy F as a function of the separation distance l for various values of the adsorption thickness $d=5$ (solid line), 10 (dotted line), 15 (dashed line), and 20 nm (dash-dotted line). The lutidine mass fraction is constant at $m_L=0.25$.

as a function of the scattering vector q to study in detail the temperature variation of the lutidine layer thickness d surrounding Stöber colloidal particles for a lutidine mass fraction $m_L=0.23$, colloidal density $c_s\sim 1.1\times 10^{12}$ cm^{-3}, and colloidal radius $R_c\sim 78$ nm. The lutidine layer was modeled as a simple slab of pure lutidine surrounding the colloidal particle; it varied from ~ 2 nm, 1.7 °C below T_a to ~ 13 nm just below T_a. From Fig. 2 in [12] we determine that the lutidine thickness increased approximately as

$$d=3.74\Delta T^{-1.29} \text{ nm}, \quad (43)$$

where $\Delta T=T_{cx}-T$ with $T_a\approx T_{cx}-0.375$ °C. At temperatures above T_a a flocculated phase formed at the bottom of the cell where the center-to-center particle separation distance r was found to be

$$r/R_c=3.0\pm 0.3 \quad (44)$$

for Stöber colloidal particles of varying size (R_c varied between 65 nm and 200 nm). The bonds between particles were thought to be liquidlike.

In order to compare our model with experiment we must examine the stability factor W [Eq. (12)] that occurs in the aggregation time t_{agg} [Eq. (11)]. The Brownian aggregation time [Eq. (10)] is readily determined to be $t_{Brown}=0.7$ s (using the parameters in Table III). In Fig. 5 we show W as a function of d. W exhibits a precipitous drop for $d\sim 10$ nm and then levels out to a constant value of ~ 0.6 corresponding to $t_{agg}\sim 0.5$ s for $d\geqslant 15$ nm. We can readily understand the region where W is constant by an examination of Fig. 4. In this region $d\gg\lambda_{D3}$ and the repulsive barrier has been screened out, thus inducing aggregation; the dispersion terms do not depend significantly on d [21]; the shape of $F(r)$ therefore does not vary much in this region and consequently W is constant. In order to determine when one would observe aggregation we must decide on a value for W, or correspondingly t_{agg}, at which aggregation would be observable. Aggregation would not be observed for a value of $W\sim 1000$ corresponding to $t_{agg}\sim 12$ min (because the system is slowly

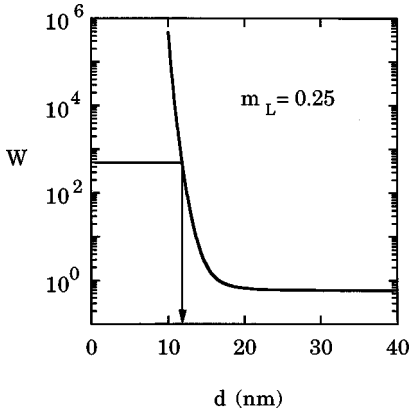

FIG. 5. Stability factor W as a function of the adsorption layer thickness d for $m_L=0.25$. In this paper we assume that aggregation is first observed when $W=500$, which corresponds to an aggregation thickness $d_{agg}\approx 12$ nm (denoted by the arrow) for this composition.

stirred to prevent gravitational settling); however, aggregation would be observed for $W\sim 100$ corresponding to $t_{agg}\sim 1$ min. Therefore, we will somewhat arbitrarily choose $W=500$ as the value at which aggregation first occurs. This value for W occurs for a lutidine adsorption layer thickness $d_{agg}\sim 12$ nm (Fig. 5) in reasonable agreement with experimental observations where $d_{agg}\sim 13$ nm [12]. We note that for this value of d there is still a large repulsive barrier for the total free energy F (Fig. 4) where the barrier height $\sim 13k_BT$.

According to our model, the colloidal particles will start to aggregate when $d\geqslant 12$ nm. What happens when the lutidine adsorption layers of two colloidal particles come into contact? The colloidal particles will be separated by a center-to-center distance of approximately $r=2R_c+24$ nm where the medium between the colloidal particles is essentially pure lutidine rather than a lutidine plus water mixture. Do the colloidal particles continue to approach each other until point contact is made or are the colloidal particles kept apart at some finite distance? We now imagine that the colloidal particles are contained within a small ''bubble'' of pure lutidine that is immersed in the lutidine-water solution (Fig. 6, inset).

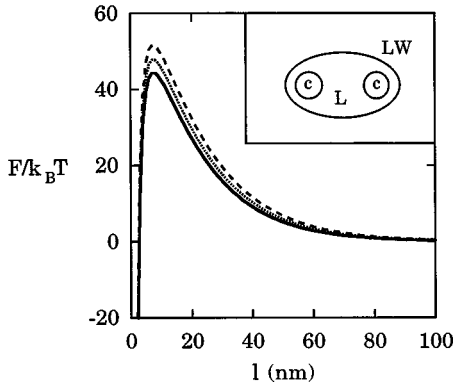

FIG. 6. Variation of the total free energy F with separation l for two colloidal particles (c) inside a lutidine ''bubble'' (L), which is surrounded by the lutidine-water mixture (LW) (see the inset). The curves represent various bubble compositions where $m_L=$ 1.00 (solid line), 0.95 (dotted line), and 0.90 (dashed line).

In order to estimate the approximate interaction free energy F between the two colloidal particles we repeat the original calculation where now the adsorption layer is absent ($d=0$) and the solvent is pure lutidine with a Debye screening length of $\lambda_{D2}=8.4$ nm. Figure 6 shows the results of this calculation. We also show on the same figure the shape of F for slight variations in the bubble composition. There is a high repulsive barrier between the colloidal particles where the maximum peak height $\sim 45k_BT$. The stability factor $W=5.6\times 10^5$ and the particles will not aggregate to point contact. Instead there will be a competition between this repulsive barrier and the energy of the bubble that surrounds the colloidal particles. The bubble energy will act like an attractive force that attempts to confine the colloidal particles in order to minimize the surface area. It is difficult to calculate the bubble energy; however, a reasonable estimate of the separation distance between colloidal particles might be where $F\approx k_BT$. This corresponds to a center-to-center separation distance of $r=2.8R_c$, which is compatible with experimental observations for the flocculated state [Eq. (44)].

Broide, Garrabos, and Beysens [14] used the time dependence of the turbidity to classify the various regimes of aggregation for systems that were quenched from an initial temperature below T_a to a final temperature above T_a. From the rate at which the turbidity increased, which is a measure of the aggregation rate, three distinctly different aggregation regimes were observed. In regime (i), where $T_a<T<T_a+0.1\,^\circ$C, the aggregation rate increased rapidly; in region (ii), where $T_a+0.1\,^\circ\text{C}<T<T_{cx}-0.1\,^\circ$C, the aggregation rate reached a plateau and was constant independent of temperature; in region (iii), where $T_{cx}-0.1\,^\circ\text{C}<T<T_{cx}$, the aggregation rate increased slightly with temperature. The aggregation dynamics was studied in detail only in region (ii), where static light scattering at various scattering vectors was measured as a function of time. These measurements were in accord with the dynamic scaling behavior of Eqs. (8) and (9) for a Brownian kernel. They determined that the mean radius of the aggregate R varied as

$$R/R_1\sim(t/t_0)^{1/3}, \tag{45}$$

where R_1 represents the monomer radius of particles that make up the aggregate and t_0 is the characteristic growth time. They also determined that the mean aggregate mass varied as

$$M\sim t. \tag{46}$$

Equations (45) and (46) imply that

$$M\sim R^{d_f}, \tag{47}$$

where $d_f=3$. In this equation d_f is the fractal dimension; a fractal dimension of 3 implies that the colloidal aggregates are compact and not fractal, namely, the bonds that hold the colloidal particles together are fluidlike, which enables the colloidal particles within the aggregate to rotate relatively freely. Broide *et al.* [14] found that if R_1 in Eq. (45) is taken to be equal to the colloidal radius R_c, then t_0 would be 5 times larger than the Brownian characteristic time given by Eq. (10). During rapid aggregation the aggregation time is similar to the Brownian limit; Broide *et al.* therefore hypoth-

esized that perhaps $R_1 = 5^{1/3} R_c$ so that the average separation distance between colloidal particles would be $\sim 3.4 R_c$. Such a separation distance would then be consistent with the flocculated phase separation distance [Eq. (44)] and would imply that this separation between colloidal particles is determined at the very beginning of the aggregation process rather than at late times when the aggregate is sizable and has settled to the bottom of the sample cell. This picture is compatible with our model for the aggregated state as encapsulated in Fig. 6. The colloidal particles can rapidly increase their separation distance within the bubble, by increasing the bubble size, because the characteristic diffusion time for lutidine to diffuse into the bubble is small (~ 60 μs).

The physical origins for the three aggregation regimes (i), (ii), and (iii), which exhibited different characteristic aggregation rates, could not be identified in [14]. From Eq. (11) for t_{agg} and Fig. 5 for W we can now surmise the origins of these three regimes. It seems probable that the adsorption layer thickness around an individual colloidal particle will still be described by Eq. (43) even above T_a. This is because although the thickness d influences F and causes aggregation above T_a, the form of F in no way influences the value of d. The value of d should merely be determined by the lutidine-water composition and the distance from T_{cx}. Region (i) where the aggregation rate increases rapidly with increasing temperature undoubtably arises from the sudden decrease in W with increasing d (Fig. 5). Aggregation is first observed when $d \sim 12$ nm and the plateau in W occurs when $d \sim 15$ nm; therefore, from Eq. (43) we can estimate the width of region (i) to be ~ 0.07 °C, which is in reasonable agreement with observations [14]. Similarly, region (ii), the plateau region where the aggregation rate is constant, most probably corresponds to the region where W is constant with a value of ~ 0.6 corresponding to an aggregation time $t_{agg} = 0.5$ s. The most difficult region to identify is region (iii), where the aggregation rate increases slightly. A possible explanation for region (iii) is that this region could mark the onset of a transition from an adsorption film to a prewetting film [38]; the slight structural change in the film could cause a change in shape to F that would register as a change in the stability factor W.

The process of fragmentation of the colloidal aggregates has also been studied [15]. The system was prepared by quenching above T_a, allowing the aggregates to grow, and then a certain time later quenching below T_a. The fragmenting of the aggregates was monitored by measuring the static light scattering at various scattering vectors. We will not describe the fragmentation of the aggregate in detail here; such processes are many-body processes and cannot readily be studied using the theoretical methods described in this paper.

C. The aggregation line

As a prelude to determining the shape of the aggregation line we have calculated the stability factor W for varying compositions and then from the criterion that $W = 500$ determined the aggregation thickness d_{agg} at each composition. In Fig. 7 we have plotted d_{agg} as a function of the lutidine mass fraction m_L. In order to be able to convert this thickness to temperature below the coexistence temperature one needs to know the adsorption thickness as a function of temperature for varying compositions.

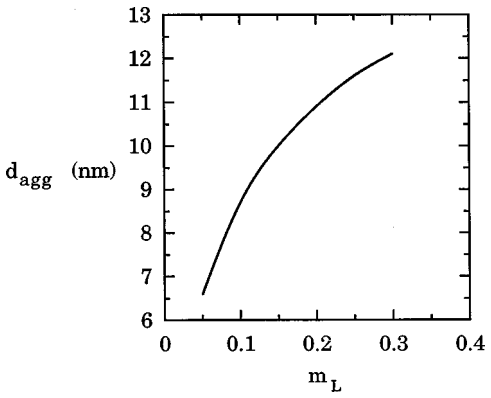

FIG. 7. Variation of the aggregation thickness d_{agg} with lutidine mass fraction m_L. The criterion $W = 500$ was used to determine d_{agg} for each m_L.

Adsorption at semi-infinite planar liquid-vapor and liquid-solid surfaces of binary liquid mixtures has been studied in many different systems [39–42]. Undoubtably this phenomenon is the same adsorption phenomenon observed at the surfaces of small colloidal particles. We expect that the adsorption thickness d will have a similar magnitude in both situations because $d \ll R_c$ and therefore studies of adsorption at semi-infinite planar surfaces should prove useful in converting the d_{agg} measurements in Fig. 7 to temperature in order that an aggregation line can be reconstructed. Perhaps the most extensive adsorption data collected at varying compositions is that of Schmidt and Moldover [40], who used Brewster angle ellipsometry to study adsorption at the liquid-vapor surface of mixtures of isopropanol (i-C_3H_7OH) and perfluoromethylcyclohexane (C_7F_{14}). The adsorption curves were very asymmetric with respect to the critical composition. A similar adsorption asymmetry has been observed by many other groups on other systems [39,42]. The component that possesses the lowest surface energy preferentially adsorbs at the surface. Adsorption is only understood extensively at the critical composition [43]. At off-critical compositions, although a theory does exist [44], it has never been compared with experimental results. Hirtz, Bonkhoff, and Findenegg [42] have developed a phenomenological theory for adsorption that appears to represent the experimental data well. We will take a very simplistic approach to the analysis of adsorption, principally because we mainly seek a qualitative understanding of the shape of the aggregation line. We therefore assume that the dielectric profile $\epsilon(z)$ that mimics the adsorption behavior a distance z from the surface can be modeled using an exponential decay

$$\epsilon(z) = (\epsilon_s - \epsilon_2) e^{-z/d_{ads}} + \epsilon_2, \tag{48}$$

where ϵ_s is the surface dielectric constant, ϵ_2 is the bulk liquid dielectric constant, and d_{ads} is the effective adsorption thickness. This profile, which is required for the analysis of the ellipsometric data, does not correctly take into account the power-law divergence that is known to exist at small distances for critical liquid mixtures [45]. However this profile has the nice property that it possesses the same effective

thickness for a given relative adsorption for both the slab profile (used in the analysis of the light scattering data) and the exponential profile (used in the analysis of the ellipsometric data). We believe that Eq. (48) will give qualitatively correct behavior as a function of composition and temperature. Brewster angle ellipsometry measures the ellipticity that is described by the Drude equation [46]

$$\bar{\rho} = \frac{\pi}{\lambda} \frac{\sqrt{\epsilon_1 + \epsilon_2}}{\epsilon_1 - \epsilon_2} \int \frac{[\epsilon(z) - \epsilon_1][\epsilon(z) - \epsilon_2]}{\epsilon(z)} dz, \qquad (49)$$

which is valid for adsorption thicknesses that are thin compared to the wavelength of light ($\lambda = 633$ nm) used in the experiment. In this expression ϵ_1 represents the optical dielectric constant of the substrate against which the adsorption occurs, for a liquid-vapor surface ($\epsilon_1 = 1$). Normally $\epsilon(z) - \epsilon_2 \ll \epsilon_2$ is a good approximation [47] and for strong adsorption, which occurs when the surface energies of the two components differ significantly, the preferentially adsorbed component is completely saturated in the first layer [48]. Then, from Eqs. (48) and (49)

$$\bar{\rho} \approx -\frac{\pi}{\lambda} \frac{\sqrt{1 + \epsilon_2}}{\epsilon_2} (\epsilon_s - \epsilon_2) d_{ads} \qquad (50)$$

and the adsorption thickness d_{ads} can readily be determined. From an analysis of the ellipsometric data of Schmidt and Moldover [40] we have determined the variation of the adsorption thickness d_{ads} as a function of the reduced composition

$$\psi = \frac{m_L - m_c}{m_c} \qquad (51)$$

for constant values of $\Delta T = T_{cx} - T$, where m_L is the mass fraction of the preferentially adsorbed component and m_c is its critical mass fraction [49]. We expect the general shape of these curves to be fairly universal independent of the particular system chosen with perhaps a multiplicative constant, related to the ratio of the correlation length amplitudes, rescaling the thickness scale. In Fig. 8 we plot d_{ads} for the lutidine-water mixture determined from the adsorption thickness calculated from the Schmidt and Moldover data scaled by $\xi_{0+}(\mathrm{LW})/\xi_{0+}(\mathrm{IP})$, where the lutidine-water correlation length amplitude $\xi_{0+}(\mathrm{LW}) = 0.25$ nm [50], while the corresponding amplitude for isopropanol-perfluoromethylcyclohexane is $\xi_{0+}(\mathrm{IP}) = 0.19$ nm [40]. From Figs. 7 and 8 we can construct an estimate of the aggregation line. Assuming that $d = d_{ads}$, then from d_{agg} (Fig. 7), for a particular m_L, we can use the smooth solid lines in Fig. 8 to determine the temperature difference $T_{cx} - T_a$. The resulting aggregation line phase diagram is shown in Fig. 9 (dashed line); the shape and position of this line would not change significantly if aggregation was assumed to occur when $W = 250$. It looks remarkably like the experimental measurements for this system (open circles) [10]. We cannot expect precise quantitative agreement between theory and experiment because of the approximations used in the ellipsometric and light scattering analysis and also because the aggregation temperature is very sensitive to the presence of any impurities in the liquid mixture [10]. The asymmetry in the aggregation line with respect to the critical composition m_c can now be attributed to the asymmetry in the adsorption behavior as a function of composition (Fig. 8).

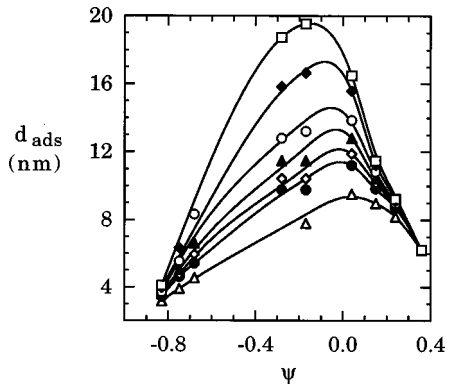

FIG. 8. Adsorption thickness d_{ads} for the lutidine-water mixture plotted as a function of the composition variable $\psi = (m_L - m_c)/m_c$ at various values of $\Delta T = T_{cx} - T$: 0.1 °C (open squares), 0.2 °C (solid diamonds), 0.4 °C (open circles), 0.6 °C (solid triangles), 0.8 °C (open diamonds), 1.0 °C (solid circles), and 2.0 °C (open triangles). See the text for a description of how d_{ads} was determined from the data of Schmidt and Moldover [40]. The smooth solid lines represent an approximate fit to the data.

D. The second virial coefficient

For temperatures below T_a additional information can be extracted from the statically scattered light extrapolated to zero scattering angle; the structure factor of such a measurement, determined in the dilute colloidal limit, gives a measure of the second virial coefficient B_2 [51]. B_2 provides corrections to the ideal gas law and is related to the interaction potential $F(l)$ between two colloidal particles [52]

$$B_2(T) = 2\pi N_A \int_{l_{min}}^{\infty} [1 - e^{-F(l)/k_B T}] l^2 dl, \qquad (52)$$

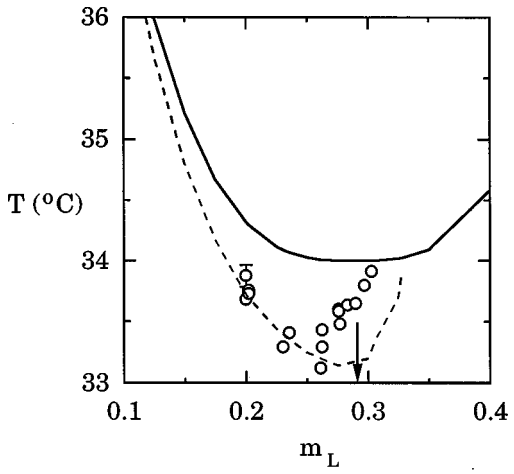

FIG. 9. Phase diagram and aggregation line for 2,6-lutidine and water containing Stöber colloidal particles. The coexistence curve is indicated by the solid line, while the dashed line is an approximate reconstruction of the colloidal aggregation line (see the text for details). The aggregation line is asymmetric with respect to the critical composition m_c (indicated by the arrow). The experimental aggregation data (open circles) are from [10].

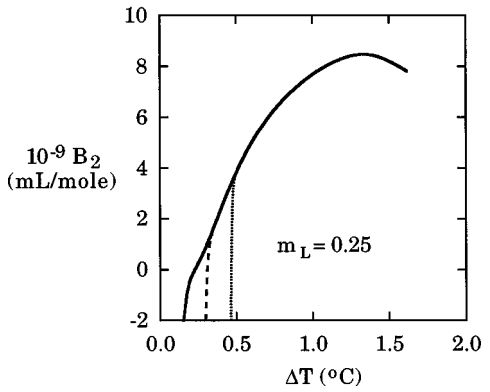

FIG. 10. Variation of the second virial coefficient B_2 as a function of $\Delta T = T_{cx} - T$ for $m_L = 0.25$. For temperatures far below T_{cx} the colloidal particles act approximately like hard spheres and B_2 acquires a value that is in approximate agreement with Eq. (53). As the temperature is increased towards T_{cx} the repulsive potential is progressively screened and B_2 decreases and eventually changes signs when the attractive dispersion interactions dominate. The change in sign of B_2 is dependent upon the value assumed for the cutoff length $l_{min} = 0.1$ (dotted line), 0.2 (dashed line), and 0.3 nm (solid line), while for larger values of ΔT the value of l_{min} is unimportant and the various curves cannot be distinguished.

where N_A is Avogadro's number, l is the separation distance between the adsorbed layers (Fig. 2), and l_{min} is a molecular cutoff at small distances that terminates the unphysical infinitely deep attractive well. For temperatures well below the aggregation temperature B_2 is expected to be positive corresponding to a repulsive barrier, where for noninteracting hard spheres of radius R_c

$$B_2 = \frac{16\pi N_A R_c^3}{3}. \tag{53}$$

As T_a is approached the repulsive barrier will decrease and the attractive interactions, which cause the aggregation, should become more dominant. Sufficiently close to T_a the second virial coefficient B_2 is expected to change sign. For the 2,6-lutidine plus water system with charged polystyrene latex colloidal particles Kurnaz and Maher [53] observed the change in sign of B_2 at a temperature $\sim 1.0\,^{\circ}\mathrm{C}$ below T_{cx}, where for their system $T_{cx} - T_a \sim 0.6\,^{\circ}\mathrm{C}$. Far from T_a they measured a value for B_2 that was a factor of 10^5 times larger than would be expected according to Eq. (53). The origin of this high repulsive barrier is not understood.

In Fig. 10 we show B_2 calculated using the model in Sec. III for $F(l)$ for various values of the cutoff parameter l_{min} [54]. In the calculation the lutidine mass fraction $m_L = 0.25$ and Eq. (43) was used to convert from adsorption thickness d to $\Delta T = T_{cx} - T$. The shape of B_2 is very similar to the experimental measurements [53] and a change in sign for B_2 is noted for sufficiently small ΔT; however, the absolute magnitude for B_2 disagrees significantly with the experimental measurements. The calculated curves for B_2 are relatively insensitive to the precise value of l_{min} for sufficiently large ΔT and their magnitude approaches the value predicted by Eq. (53), $B_2 = 1 \times 10^{10}$ mL/mole for $R_c = 100$ nm. At small values of ΔT the shape of B_2 is very sensitive to the cutoff parameter l_{min}.

V. SUMMARY

A quantitative theoretical explanation for adsorption-induced reversible colloidal aggregation, in certain types of binary liquid mixtures, has been lacking since its observation by Beysens and Estève in 1985 [7]. In another work [21] we extended the traditional Derjaguin-Landau-Verwey-Overbeek theory for colloidal aggregation [22] by modeling the attractive potential using the more realistic Dzyaloshinskii-Lifshitz-Pitaevskii theory for dispersion interactions [23] and by including the effects of an adsorbed layer in the attractive and repulsive potentials. We demonstrated that the primary effect of the adsorbed layer was to produce a Debye screening length within the adsorbed layer λ_{D3}, which in general differed from the Debye screening length in the bulk solution λ_{D2}. This screening length predominantly influenced the electrostatic repulsive potential and progressively screened this potential as the adsorption thickness d increased.

We have extended these calculations in this paper to other aspects connected with adsorption-induced colloidal aggregation and where possible compared theory with experimental observations. The most detailed experiments have been performed on mixtures of 2,6-lutidine plus water containing Stöber colloidal particles for a lutidine mass fraction $m_L \approx 0.25$. The theory indicates that the decreasing repulsive barrier with increasing adsorption layer thickness d is the primary cause for the observation of colloidal aggregation. We find reasonable agreement between theory and experiment for the adsorption thickness d_{agg} at which aggregation first occurs. The theory is able to explain the reason for the fluidlike bonds between the colloidal particles in the aggregated state where the average center-to-center colloidal separation distance r is approximately three times the colloidal radius R_c. The shape of the stability factor W with increasing d (Fig. 5) explains the separation in the aggregation dynamics into a rapidly varying aggregation rate where W decreases precipitously [region (i)] and a region with a constant aggregation rate where W is constant [region (ii)]. A detailed study of region (i) should prove a profitable area for future experimental research because the precise variation of the aggregation rate with temperature is closely connected with the shape of the total free energy F via Eq. (12). The theory has also provided an explanation for the asymmetric shape of the aggregation line with respect to the critical composition (Fig. 9); the asymmetric shape is related to the adsorption asymmetry that has frequently been observed at semi-infinite binary liquid-substrate surfaces [39,40,42]. The thermal variation of the second virial coefficient B_2 (Fig. 10) is similar in shape to the experimental measurements [53] and also gives agreement with the hard-sphere value [Eq. (53)] for temperatures sufficiently far below the aggregation temperature T_a.

There are still a number of unresolved problems. In the Introduction we noted a surface charge effect where for small colloidal surface charge densities the aggregation line occurred on the lutidine-poor side of the phase diagram [Fig.

1(a)] while for high colloidal surface charge densities it occurred on the lutidine-rich side of the phase diagram [Fig. 1(b)]. In these two cases the adsorbed layer consisted of lutidine or water, respectively. This surface charge effect may be related to the solubility of the colloids; from the discussion in [20] we speculate that perhaps colloids with large surface charge densities are more soluble in solvents of higher static dielectric constant. Such an effect would determine the composition of the adsorbed layer and hence also the positioning of the aggregation line on the phase diagram. van Duijneveldt and Beysens [13] demonstrated an intimate connection between the lutidine layer thickness and the aggregation line. They observed that when Mg^{2+} ions were added to solution, by the addition of small amounts of $Mg(NO_3)_2$, the formation of an adsorbed layer of lutidine was suppressed and even reversed into the formation of a layer of water for sufficiently large amounts of the salt. At the same time $T_{cx}-T_a$ decreased with increasing salt concentration and decreasing lutidine layer thickness and the reversible aggregation completely disappeared with the disappearance of the lutidine adsorption layer. At this time it is difficult to quantitatively interpret this phenomenon using our adsorption-induced model of aggregation because no detailed theoretical studies have been made of how the presence of salt influences the adsorption layer thickness; additionally, the relative solubility of the salt in the adsorbed layer compared to the bulk medium is not understood. Narayanan *et al.* [15] have completed extensive studies of the fragmentation of the colloidal aggregates by quenching an aggregate from above T_a to below T_a while monitoring the redispersing of the colloidal particles into the solvent medium using static light scattering. This is a many-body problem and therefore cannot be readily handled with the techniques used in this paper; however, a computer simulation with the potential energy of the interaction given in Sec. III between the colloidal particles may be able to determine whether or not this potential is consistent with the experimental observations of fragmentation.

We expect adsorption-induced aggregation to be quite common in nature and to occur in situations where surface active minority or impurity components have an enhanced solubility for charged species, relative to the bulk solution, thus giving rise to a different Debye screening length in the adsorption layer. If these charged species are of opposite sign to the colloidal surface charge then the repulsive potential will be screened and aggregation may occur for a sufficiently thick adsorption layer of the order of a few nanometers. This phenomenon could be the explanation for some puzzling experimental results [55] where evidence for an additional attractive interaction was obtained in a regime where the repulsive potential was expected to dominate.

ACKNOWLEDGMENTS

B. M. L. would like to thank colleagues at CEA, DRFMC, Grenoble for their kind hospitality and financial support during his brief stay when many of the ideas in this publication were finalized. He would also like to thank Dr. D. Frenkel, Dr. A. van Blaaderen, Professor R. Evans, and Professor S. Dietrich for useful discussions. B. M. L. acknowledges support for this work under NSF Grant No. DMR-9631133.

[1] *Coagulation and Flocculation*, edited by B. Dobiáš, Surfactant Science Series No. 47 (Dekker, New York, 1993).
[2] J. C. Crocker and D. G. Grier, Phys. Rev. Lett. **73**, 352 (1994).
[3] *On Growth and Form—Fractal and Non-Fractal Patterns in Physics*, Vol. 100 of *NATO Advanced Study Institute, Series E: Applied Science*, edited by H. E. Stanley and N. Ostrowsky (Nijhoff, Dordrecht, 1986).
[4] K. Schätzel and B. J. Ackerson, Phys. Rev. Lett. **68**, 337 (1992).
[5] C. A. Murray and D. H. Van Winkle, Phys. Rev. Lett. **58**, 1200 (1987).
[6] W. B. Russel, D. A. Saville, and W. R. Schowalter, *Colloidal Dispersions* (Cambridge University Press, Cambridge, 1989).
[7] D. Beysens and D. Estève, Phys. Rev. Lett. **54**, 2123 (1985).
[8] For a review see D. Beysens, J.-M. Petit, T. Narayanan, A. Kumar, and M. Broide, Ber. Bunsenges. Phys. Chem. **98**, 382 (1994).
[9] P. D. Gallagher and J. V. Maher, Phys. Rev. A **46**, 2012 (1992); P. D. Gallagher, M. L. Kurnaz, and J. V. Maher, *ibid.* **46**, 7750 (1992).
[10] T. Narayanan, A. Kumar, E. S. R. Gopal, D. Beysens, P. Guenoun, and G. Zalczer, Phys. Rev. E **48**, 1989 (1993).
[11] Y. Jayalakshmi and E. W. Kaler, Phys. Rev. Lett. **78**, 1379 (1997).
[12] V. Gurfein, D. Beysens, and F. Perrot, Phys. Rev. A **40**, 2543 (1989).
[13] J. S. van Duijneveldt and D. Beysens, J. Chem. Phys. **94**, 5222 (1991).
[14] M. L. Broide, Y. Garrabos, and D. Beysens, Phys. Rev. E **47**, 3768 (1993).
[15] T. Narayanan, J.-M. Petit, M. L. Broide, and D. Beysens, Phys. Rev. E **51**, 4580 (1995).
[16] H. T. Dobbs and J. M. Yeomans, J. Phys.: Condens. Matter **4**, 10 133 (1992).
[17] H. Löwen, Phys. Rev. Lett. **74**, 1028 (1995).
[18] T. W. Burkhardt and E. Eisenriegler, Phys. Rev. Lett. **74**, 3189 (1995); R. R. Netz, *ibid.* **76**, 3646 (1996).
[19] T. J. Sluckin, Phys. Rev. A **41**, 960 (1990).
[20] J. N. Israelachvili, *Intermolecular and Surface Forces*, 2nd ed. (Academic, London, 1992).
[21] J.-M. Petit, B. M. Law, and D. Beysens, J. Colloid Interface Sci. (to be published).
[22] E. J. W. Verwey and J. Th. G. Overbeek, *Theory of the Stability of Lyophobic Colloids* (Elsevier, New York, 1948).
[23] I. E. Dzyaloshinskii, E. M. Lifshitz, and L. P. Pitaevskii, Adv. Phys. **10**, 165 (1961); J. Mahanty and B. W. Ninham, *Dispersion Forces* (Academic, London, 1976).
[24] L. A. Spielman, J. Colloid Interface Sci. **33**, 562 (1970).
[25] J. Th. G. Overbeek, in *Colloid Science*, edited by H. R. Kruyt (Elsevier, Amsterdam, 1952), Vol. 1.
[26] P. G. J. van Dongen and M. H. Ernst, Phys. Rev. Lett. **54**, 1396 (1985).

[27] N. Fuchs, Z. Phys. **89**, 736 (1934).
[28] E. P. Hong, G. J. Roebersen, and P. H. Wiersema, J. Colloid Interface Sci. **36**, 97 (1971).
[29] B. A. Pailthorpe and W. B. Russel, J. Colloid Interface Sci. **89**, 563 (1982).
[30] D. B. Hough and L. R. White, Adv. Colloid Interface Sci. **14**, 3 (1980).
[31] V. A. Parsegian and B. W. Ninham, Nature (London) **224**, 1197 (1969); B. W. Ninham and V. A. Parsegian, Biophys. J. **10**, 646 (1970); J. Chem. Phys. **52**, 4578 (1970); V. A. Parsegian and B. W. Ninham, Biophys. J. **13**, 209 (1973).
[32] R. F. Kayser, Phys. Rev. B **34**, 3254 (1986).
[33] D. Gingell and V. A. Parsegian, J. Theor. Biol. **36**, 41 (1972).
[34] A. Stein, S. J. Davidson, J. C. Allegra, and G. F. Allen, J. Chem. Phys. **56**, 6164 (1972).
[35] J. V. Sengers, Int. J. Thermophys. **6**, 203 (1985).
[36] V. Gurfein, Ph.D. thesis, Universite Paris VI, 1989 (unpublished), p. 122.
[37] C. Kittel and H. Kroemer, *Thermal Physics*, 2nd ed. (Freeman, New York, 1980).
[38] P. Taborek and J. E. Rutledge, Phys. Rev. Lett. **68**, 2184 (1992); J. E. Rutledge and P. Taborek, *ibid.* **69**, 937 (1992); H. Kellay, D. Bonn, and J. Meunier, *ibid.* **71**, 2607 (1993).
[39] A. I. Rusanov and V. I. Pshenitsyn, Dokl. Akad. Nauk SSSR **187**, 619 (1969) [Dokl. Phys. Chem. **187**, 509 (1969)]; D. Beaglehole, J. Chem. Phys. **73**, 3366 (1980).
[40] J. W. Schmidt and M. R. Moldover, J. Chem. Phys. **83**, 1829 (1985); **84**, 4563 (1986).
[41] M. Privat, L. Tenebre, R. Bennes, E. Tronel-Peyroz, J. M. Douillard, and L. Ghaicha, Langmuir **4**, 1151 (1988).
[42] A. Hirtz, K. Bonkhoff, and G. H. Findenegg, Adv. Colloid Interface Sci. **44**, 241 (1993).
[43] See D. S. P. Smith, B. M. Law, M. Smock, and D. P. Landau, Phys. Rev. E **55**, 620 (1997), and references therein.
[44] D. Beaglehole, J. Chem. Phys. **75**, 1544 (1981).
[45] M. E. Fisher and P.-G. de Gennes, C. R. Acad. Sci. Paris B **287**, 207 (1978); H. Zhao, A. Penninckx-Sans, L.-T. Lee, D. Beysens, and G. Jannink, Phys. Rev. Lett. **75**, 1977 (1995).
[46] P. K. L. Drude, *The Theory of Optics* (Dover, New York, 1959), p. 292.
[47] B. M. Law, Phys. Rev. Lett. **67**, 1555 (1991).
[48] D. S. P. Smith and B. M. Law, Phys. Rev. E **54**, 2727 (1996).
[49] In the analysis of the Schmidt and Moldover data [40] we have assumed that the ellipticity $\overline{\rho}$ at the closest approach to the coexistence curve is 0.1 °C from T_{cx}.
[50] E. Gulari, A. F. Collings, R. L. Schmidt, and C. J. Pings, J. Chem. Phys. **56**, 6169 (1972). We have used the mean value of the two correlation length amplitudes measured by these authors.
[51] A. P. Philipse and A. Vrij, J. Chem. Phys. **88**, 6459 (1988).
[52] J. P. Hansen and I. R. McDonald, *Theory of Simple Liquids* (Academic, London, 1976).
[53] M. L. Kurnaz and J. V. Maher, Phys. Rev. E **51**, 5916 (1995); **55**, 572 (1997).
[54] Great care must be taken in the numerical integration of B_2 because the exponential term is extremely sensitive to the attractive part of $F(l)$. The integral was subdivided into two regions; the small-l region from l_{min} to l_0 was calculated using 64-point Gaussian-Legendre integration while the large-l region from l_0 to ∞ was calculated using 56-point Gaussian-Laguerre integration. Here l_0 corresponds to the separation distance at which $F(l_0)=0$.
[55] B. V. R. Tata, M. Rajalakshmi, and A. K. Arora, Phys. Rev. Lett. **69**, 3778 (1992); **72**, 787 (1994); T. Palberg and M. Würth, *ibid.* **72**, 786 (1994).
[56] R. W. Rampolla and C. P. Smyth, J. Am. Chem. Soc. **80**, 1057 (1958).
[57] D. P. Biddiscombe, E. A. Coulson, R. Handley, and E. F. G. Herington, J. Chem. Soc. (London) **1954**, 1957 (1954).
[58] V. P. Parsegian and G. H. Weiss, J. Colloid Interface Sci. **62**, 344 (1977).
[59] C. Houessou, Ph.D. thesis, Universite Paris VII, 1986 (unpublished).